Heat transfer predictions in cavities

By A. Ooi, G. Iaccarino AND M. Behnia[1]

1. Motivations & objectives

Artificial roughness elements (ribs) introduced in flow passages is a popular method of enhancing heat transfer in the cooling passage of turbine blades, heat exchangers etc. It is essential to accurately predict the enhancement of heat transfer generated by the roughness elements to ensure good design decisions. Experimental studies have been carried out by various investigators e.g. Han *et al.* (1978), Han (1984), Han *et al.* (1985), Han (1988), Chyu & Wu (1989), Korotky & Taslim (1998), and Rau *et al.* (1998). It has been found that the conventional $k-\epsilon$ turbulence models with wall functions do not accurately predict the data (Simoneau 1992) for this geometrical configuration. This is mainly because the flow field has both separation and reattachment points, and it is well known that the $k-\epsilon$ model with wall functions leads to erroneous predictions for this situation. In order to obtain better predictions, Liou *et al.* (1993) performed two-dimensional numerical simulations using a $k-\epsilon-A$ algebraic stress and heat flux model. Good agreement with experimental data were obtained, but extension of the method to three dimensions is computationally expensive and could lead to equations that are numerically stiff (Gatski & Speziale 1993 and Speziale 1997).

Stephens & Shih (1995) used the $k-\omega$ model to compute three-dimensional ribbed channel with heat transfer and compared their results with experimental data of Chyu & Wu (1989). They achieved good qualitative but not quantitative agreement. More recently, Iacovides (1998) showed that two layer $k-\epsilon$ with the Wolfshtein (1969) one-equation near-wall model for k transport gives unsatisfactory heat transfer predictions in rotating ribbed passages. Better results were obtained by employing a low-Re version of a differential stress model. However, this model is computationally expensive and only achieved marginal improvement in heat transfer predictions.

The v^2-f turbulence model was introduced by Durbin (1991) and has been successfully used to predict heat transfer in attached boundary layers and channel flows (Durbin 1993). This model was later used by Behnia *et al.* (1997) to predict heat transfer in an axisymmetric impinging jet. The impinging jet is a very challenging test case because the applications of traditional turbulence models to this flow configuration have been shown to result in poor agreement with available experimental data. Computations using the v^2-f model give better heat transfer predictions in this axisymmetric two-dimensional environment. Here, the v^2-f

1 Current address: Dept. of Mechanical and Manufacturing Engr., University of New South Wales, NSW 3052, Australia

turbulence model will be used in a three-dimensional domain to test its ability to predict heat transfer in ribbed passages. We will compare results of the current simulation with the experimental data of Rau *et al.* (1998).

Also of interest is the prediction of heat transfer in a geometry resembling the clearance gap between the tip of an axial turbine blade tip and the adjacent stationary shroud. This problem is of great interest in the engineering community because heat transfer at the blade tip can give rise to large temperature gradients, which in turn causes durability problems. Booth *et al.* (1982) and Wadia & Booth (1982) have investigated the aerodynamic characteristics of this narrow flow passage between the pressure and suction sides of the blade. Metzger *et al.* (1989) have provided experimental heat transfer data for this configuration, and we will compare the $v^2 - f$ heat transfer predictions with this data.

2. Accomplishments

2.1 Turbulence models

Most of the results presented below are obtained using the $v^2 - f$ turbulence model. It is computationally more expensive than the conventional $k-\epsilon$ model but is relatively inexpensive compared to algebraic stress and full second moment closure models. The equations for this model can be found in various publications (Behnia 1997, Lien & Durbin 1996) and will not be repeated here. The temperature field is obtained by assuming a constant turbulent Prandtl number, $Pr_t = 0.9$, relating the eddy diffusivities of heat and momentum; i.e. the turbulent heat flux is simply approximated as

$$\langle u_i \theta \rangle = -\frac{\nu_t}{Pr_t} \frac{\partial \Theta}{\partial x_i},$$

where ν_t is the eddy viscosity and Θ is the mean temperature. As will be discussed later, this approximation is only valid for forced convection problems. More complicated models for $\langle u_i \theta \rangle$ are needed where buoyancy effects are significant.

To highlight the advantages of $v^2 - f$ over the more commonly used $k-\epsilon$ model, similar numerical computations were also performed with a $k-\epsilon$ model. For these simulations, the conventional $k-\epsilon$ model matched to the low-Re $k-l$ model proposed by Wolfshtein (1969) is used. This wall-treatment is chosen because it is the default 2 layer model used in many commercial CFD packages.

2.2 Computational domain, parameters, and boundary conditions

Two different sets of computations will be considered in this paper. The first set is the ribbed channel; the corresponding computational domain is shown in Fig. 1. To minimize the number of grid points, symmetry of the mean flow is assumed at the mid-channel. Numerical simulations were carried out with the ribs placed on one wall (1s) or on two opposite walls (2s). For the 2s simulations, symmetric boundary conditions were used on the top of the computational domain, and for the 1s simulations, the no-slip condition is used. The flow is assumed to be fully developed, hence the velocity field is periodic in the streamwise direction. For these

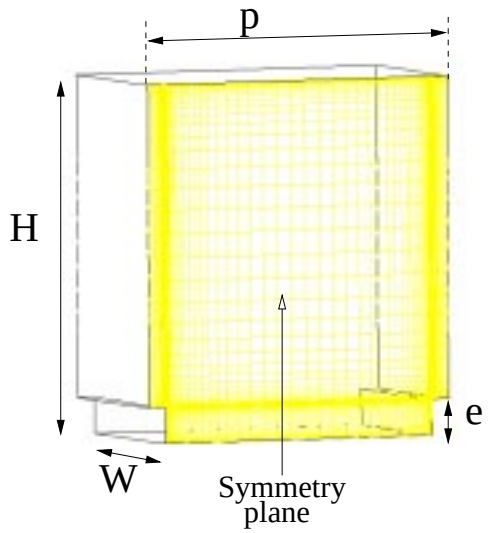

FIGURE 1. Three-dimensional computational domain for ribbed passage simulations.

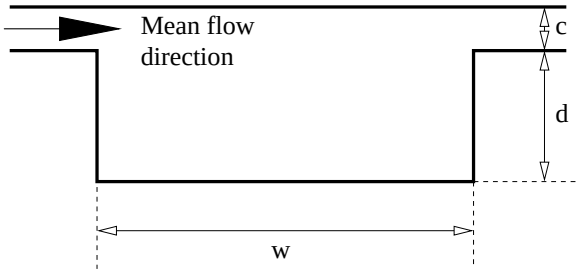

FIGURE 2. Two-dimensional computational domain for blade tip simulations.

simulations the rib height-to-channel hydraulic diameter ratio is fixed at $e/D_h = 0.1$, where the hydraulic diameter, D_h, is defined to be

$$D_h = \frac{2WH}{W+H}.$$

Channel width-to-height ratio (W/H) is unity. Simulations were carried out with different pitch to rib-height ratios of

$$p/e = 6, 9, 12.$$

All Nusselt number distributions for the ribbed channel calculations presented here are normalized with respect to the level obtained in a smooth circular tube (i.e. Dittus-Boelter correlation)

$$Nu_0 = 0.023 Re^{0.8} Pr^{0.4}.$$

The Reynolds number is

$$Re = \frac{U_{bulk} D_h \rho}{\mu} = 30,000$$

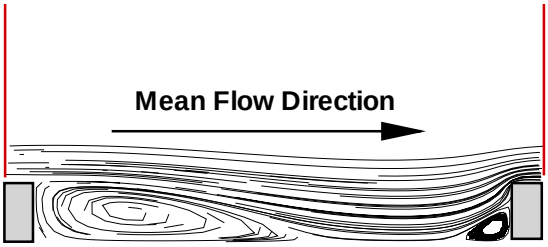

FIGURE 3. Flow pattern on the symmetry plane of the computational domain.

where the bulk velocity, U_{bulk}, is defined as

$$U_{bulk} = \frac{\dot{m}}{\rho A_c}.$$

A_c is the cross-sectional area of the passage. The molecular Prandtl number, $Pr = 0.71$, is kept constant for all simulations. For heat transfer calculations, a constant heat flux is applied at the walls.

All results presented here are from simulations with $81(x) \times 65(y) \times 31(z)$ grid points. To ensure that the results are independent of the grid, all simulations were repeated with twice the number of grid points in each spatial direction. No noticeable difference in the solutions were observed, hence the solutions presented here are assumed to be grid independent.

The other problem considered is a model for the grooved turbine blade tip cross section. This configuration is shown in Fig. 2. The mean flow field in the experiments by Metzger *et al.* (1989) is essentially two-dimensional at Reynolds number

$$Re = \frac{\rho U_{bulk} C}{\mu} = 1.5 \times 10^4.$$

The ratio of clearance height to cavity width, c/w, was fixed at 0.1 and two different

$$d/w = 0.1, 0.2$$

ratios were considered. Constant temperature boundary conditions are used for all walls and the Prandtl number, Pr, is kept constant at 0.71. Nusselt number distribution on the cavity floor will be compared with the experimental data of Metzger *et al.* (1989).

2.3 Results and discussion (ribs)

Figure 3 shows the flow pattern on the symmetry plane of the computational domain. The flow separates after going over the upstream rib creating a low pressure region behind the rib. Further downstream, the flow reattaches and forms a short recovery region downstream of the reattachment point. This flow then impinges on the next rib, forming a small recirculating region in front of the downstream rib. The flow pattern just described is difficult to model mainly because it contains

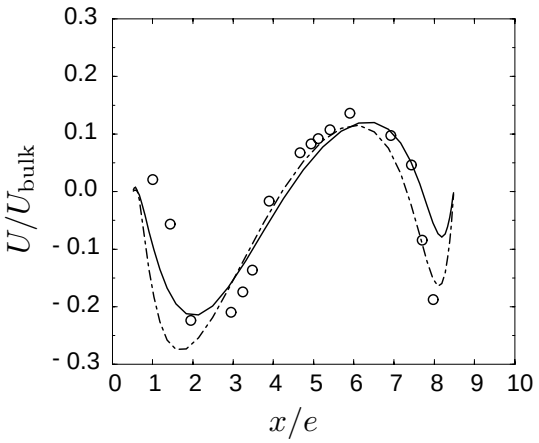

FIGURE 4. Comparison of the streamwise velocity component, U, at $y/e = 0.1$ on the symmetry plane of the computational domain. This figure shows data from a 1s simulation with $p/e = 9$. ——— $v^2 - f$ turbulence model, —·— $k - \epsilon$ 2 layer model, ∘ experimental data of Rau *et al.* (1998).

both separation and reattachment points. Parneix & Durbin (1996) have used the $v^2 - f$ model to accurately predict the reattachment point and the downstream recovery region of a backstep flow. Analysis of the data here will determine if $v^2 - f$ can predict the short recovery region and the subsequent separation point before the downstream rib. Figure 4 shows the streamwise velocity distribution close to the floor (10% of the rib height) between the two ribs on the symmetry plane. As can be seen, both the $k - \epsilon$ and $v^2 - f$ models accurately predict the separation and reattachment points. The velocity maximum and minimum in the recovery and reverse flow region are more accurately predicted by the $v^2 - f$. The $k - \epsilon$ model predicts a more accurate minimum streamwise component of velocity in the recirculating bubble just before the downstream rib.

Heat transfer predictions from the $v^2 - f$ and $k - \epsilon$ models are shown in Fig. 5. The comparisons are for the 2s simulations with $p/e = 9$. As can be seen, heat transfer predicted by the $k - \epsilon$ model is roughly half the heat transfer measured in the experiment. Calculations by Iacovides (1998) utilizing the same $k - \epsilon$ low Re number model and using a different p/e and e/D_h ratio also shows that the $k - \epsilon$ model predicts a Nusselt number distribution of about half the actual experimental data. Since his calculations were computed for a rotating channel with different geometrical ratios, using a different numerical method and different types of grids, there can be no numerical issues in the discrepancies between the $k - \epsilon$ predictions and experimental data.

In addition, Iacovides (1998) also calculated the flow using a Reynolds stress model which is computationally more expensive than $v^2 - f$. The Nusselt number predicted by the Reynolds stress model was better than the $k - \epsilon$ calculations. Figure 5 indicates that the $v^2 - f$ model yields very good agreement with experimental values.

In Fig. 6, heat transfer predictions using $v^2 - f$ for different geometrical ratios

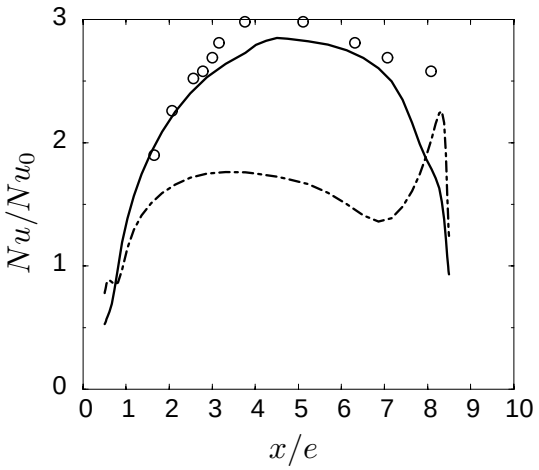

FIGURE 5. Comparison of the Nusselt number distribution for the 2-sided ribbed channel with $p/e = 9$ on the symmetry plane of the computational domain. ——— $v^2 - f$ turbulence model, —– – $k - \epsilon$ 2 layer model, ∘ experimental data of Rau *et al.* (1998).

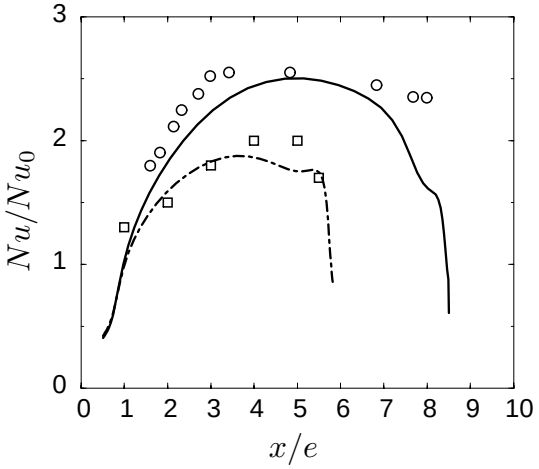

FIGURE 6. Nusselt number distribution on the floor of the symmetry plane. ——— $v^2 - f$ with 1s $p/e = 9$, ∘ corresponding experimental data from Rau *et al.* (1998), —– – $v^2 - f$ with $p/e = 6$, ▫ corresponding experimental data from Rau *et al.* (1998).

are compared with the corresponding data from Rau *et al.* (1998). Experimental data show that the heat transfer rate decreases with p/e ratio. The $v^2 - f$ model accurately reproduces this observation, both qualitatively and quantitatively. The $k-\epsilon$ calculations are not shown in this figure, but the predictions are about half the values obtained from the experiments. This is illustrated in Fig. 7, which shows the average Nusselt number on the floor between the two ribs for different p/e ratios computed here. The results show that the $k - \epsilon$ model consistently underpredicts the heat transfer on the floor between the two ribs. The $v^2 - f$ results are better but still lower than the experimental data.

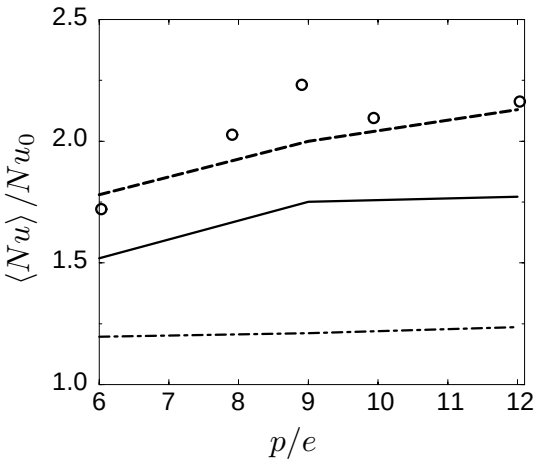

FIGURE 7. Average Nusselt number on the floor of the computational domain. —— $v^2 - f$, - - - - $v^2 - f$ for "reduced" domain, — - — $k - \epsilon$, ∘ experimental data from Rau *et al.* (1998).

It must be pointed out that the $v^2 - f$ results shown by the solid line in Fig. 7 are the Nusselt numbers averaged over the whole area between the two ribs. Careful observation of the experimental data shown in Figs. 5 and 6 indicates the first and last experimental data points are approximately $0.5e$ away from the upstream and downstream ribs respectively. The Nusselt number is quite low in the region close to the ribs, and this brings down the average. Thus, a more accurate comparison with experimental data would be to average Nu only in areas where experimental data exist. We are currently in the process of obtaining these experimental data from the group at Von Karman Institute where the experiment was carried out. However, if the Nu was calculated using only an area which is $0.5e$ away from the ribs and $1.0e$ away from the side walls, there is very good agreement between the $v^2 - f$ results and the experimental data. This is shown by the dashed line in Fig. 7.

Figure 8 shows the local Nusselt number distribution for both models on the side wall. The maximum Nusselt number on the side wall is located at the first corner of the downstream rib. The highest contour level for Nu/Nu_0 using the $k - \epsilon$ model is 2.2 and for the $v^2 - f$ model is 2.0. Experimental data shows that the maximum contour level is 2.24. This initial observation might lead one to believe that the $k - \epsilon$ model gives better prediction on the side wall. A better way of determining the performance of the models will be to compare the average Nusselt numbers on the side wall. These data are shown in Fig. 9, and the $v^2 - f$ prediction is closer to the experimental data. However, it is clear that the side wall predictions are not as good as the predictions for the wall between the ribs. Future studies will attempt to find the source of this discrepancy. Similar to the data on the wall between the ribs, there can be better agreement with experimental data if one averages only within the area away from the corners of the computational domain. This is not done for the side wall because it is unclear from the paper by Rau *et al.* (1998) how close to the corners the experimental data on the side wall were taken. We are currently in the process of obtaining this information.

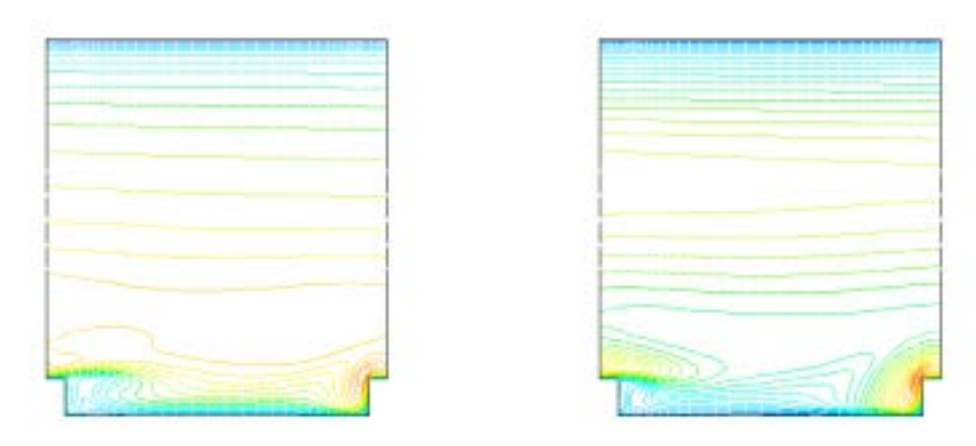

FIGURE 8. Nusselt number contours on the smooth side wall of the computational domain computed using $v^2 - f$ turbulence model (contour level is 0.3–2.0) (left) and $k - \epsilon$ turbulence model (contour level is 0.3–2.2) (right).

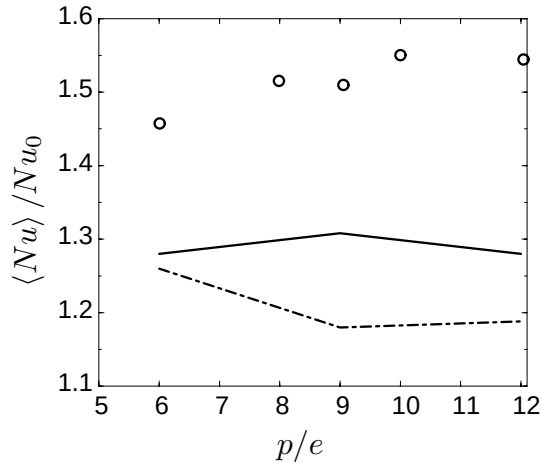

FIGURE 9. Average Nusselt number on the smooth side wall of the computational domain. ——— $v^2 - f$, — - — $k - \epsilon$, ∘ experimental data from Rau *et al.* (1998).

2.4 Results and discussion (blade tip)

The second set of simulations were performed to investigate the ability of the $v^2 - f$ model to predict heat transfer at the tip of a turbine blade. The resulting flow fields for $d/w = 0.1$ and $d/w = 0.2$ are shown in Fig. 10. For $d/w = 0.1$, the flow pattern is very similar to the one shown in Fig. 3. The flow separates at wall A and reattaches on the floor. In the case of $d/w = 0.2$, the flow pattern changes and the flow separates as it leaves wall A and reattaches, not on the floor, but on the side of wall B. There is a slow mean recirculating region between walls A and B similar to the driven cavity flow.

The heat transfer predictions on the floor between the two walls are shown in Fig. 11. Similar to the case of the ribbed channel, the Nusselt number distribution predicted by the $k - \epsilon$ model is too low. On the other hand, $v^2 - f$ gives good agreement with experimental data. The agreement with experimental data is better

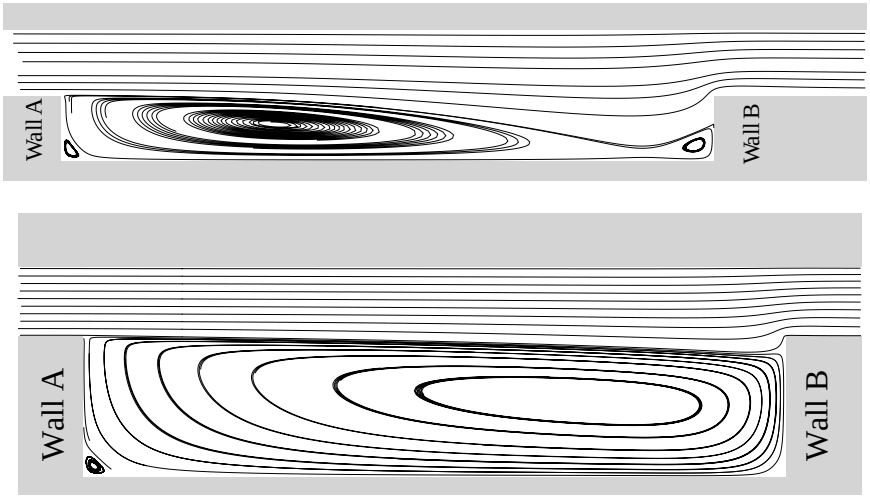

FIGURE 10. Flow pattern for blade tip flow simulation using the $v^2 - f$ turbulence model. The figure on the top is for $d/w = 0.1$ and the figure on the bottom is for $d/w = 0.2$.

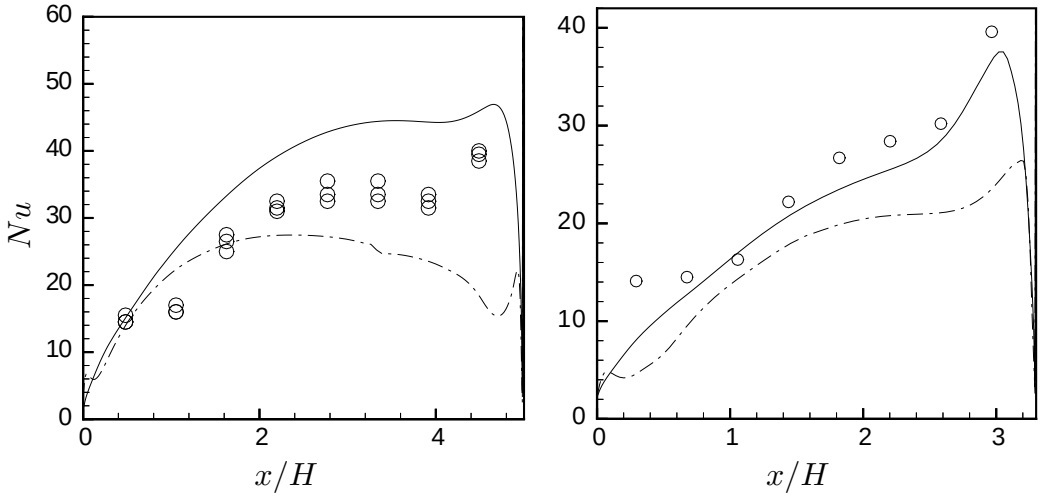

FIGURE 11. Nusselt number distribution on the floor for $d/w = 0.1$ (left) and $d/w = 0.2$ (right). —— $v^2 - f$, — - — $k - \epsilon$, ∘ experimental data of Metzger *et al.* (1989). The experiment was repeated with three different inlet temperatures and all measured data sets are shown in this figure.

for the flow with $d/w = 0.2$ than $d/w = 0.1$. It is interesting to note that the experimental data with $d/w = 0.1$ shows a peak in the Nusselt number close to wall B. The $v^2 - f$ model reproduces this peak whereas data using the $k - \epsilon$ model shows a dip in the heat transfer.

Calculations were also carried out to assess the accuracy of using wall functions with the $k - \epsilon$ model. The computations were done using a similar mesh to the previous calculations. As wall functions are really only valid for approximately $y^+ > 30$, the grid needs to be coarsened so that wall functions can be used. Grid

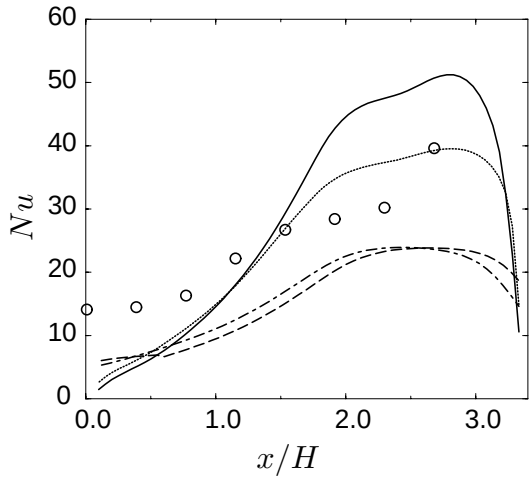

FIGURE 12. Nusselt number distribution on the floor for $d/w = 0.2$. Calculations performed with $k-\epsilon$ model with standard wall functions.—— $y^+ \simeq 3$, ····· $y^+ \simeq 5$,—— y^+---- 30, —·— $y^+ \simeq 50$, ∘ experimental data of Metzger *et al.* (1989).

lines closest to the floor were removed to ensure the distance from the first grid line to the wall is increased. Four meshes were generated corresponding to average y^+ along the cavity floor ranging from approximately 3 to about 50. Results from these calculations are shown in Fig. 12 and compared with the experimental data. As expected, the results are grid dependent for $y^+ < 30$, but surprisingly, the calculations agree quite well with experimental data when $y^+ \approx 3$ or 5. When $y^+ \approx 30$ or 50, the Nusselt number is underpredicted. In this case, the wall function is a bit worse than the two layer model. This is despite the fact that there is a slow recirculation region, and it is questionable whether a log law exists close to the wall of the cavity.

3. Future plans

The results above and computations by Durbin (1993) and Behnia *et al.* (1997) show that the heat transfer predictions by the $v^2 - f$ turbulence model agree very well with experimental data. To this end, the model has only been tested in a forced convection environment, and it has been shown that the simple gradient diffusion hypothesis with a constant turbulent Prandtl number is sufficient to obtain good agreement with experimental data. However, buoyancy effects are not included in the current model, hence $v^2 - f$ cannot be expected to give good predictions in situations where buoyancy plays an important role. Assuming that the Boussinesq approximation holds, the source term due to gravity in the Reynolds stress transport equation becomes

$$-\beta g_i \langle u_j \theta \rangle - \beta g_j \langle u_i \theta \rangle .$$

Thus, to accurately model buoyancy effects, a good model for the turbulence heat flux, $\langle u_i \theta \rangle$, is needed. Future work will explore the feasibility of incorporating buoyancy effects into $v^2 - f$ by extending the algebraic heat flux analysis of Shabany & Durbin (1997).

REFERENCES

Behnia, M., Parneix, S. & Durbin, P. 1997 Accurate modeling of impinging jet heat transfer". *CTR Annual Research Briefs,* NASA Ames/Stanford Univ., 149-164.

Booth, T. C., Dodge, P. R. & Hepworth, H. K. 1982 Rotor-Tip Leakage:Part I-Basic Methodology. *ASME J. Engr. for Power.* **104,** 154-161.

Chyu, M. K. & Wu, L. X. 1989 Combined effects of rib angle-of-attack and pitch-to-height ratio on mass transfer from a surface with transverse ribs. *Exp. Heat Transfer.* **2,** 291-308.

Durbin, P. A. 1991 Near-Wall Turbulence Closure Modeling Without "Damping Functions". *Theor. and Comp. Fluid Dynamics.* **3,** 1-13.

Durbin, P. A. 1993 Application of a near-wall turbulence model to boundary layers and heat transfer. *Int. J. Heat and Fluid Flow.* **14**(4)**,** 316-323.

Gatski, T. B. & Speziale, C. G. 1993 On explicit algebraic stress models for complex turbulent flows. *J. Fluid Mech.* **254,** 59-78.

Han, J. C., Glicksman, L. R. & Rohsenow W. M. 1978 An investigation of heat transfer and friction for rib-roughened surfaces. *Int. J. Heat Mass Transfer.* **21,** 1143-1156.

Han, J. C. 1984 Heat Transfer and Friction in Channels With Two Opposite Rib-Roughened Walls. *J. Heat Transfer.* **106,** 774-781.

Han, J. C., Park, J. S. & Lei, C. K. 1985 Heat Transfer Enhancement in Channels With Turbulence Promoters. *J. of Engr. for Gas Turbines and Power.* **107,** 628-635.

Han, J. C. 1988 Heat Transfer and Friction Characteristics in Rectangular Channels with Rib Turbulators. *J. Heat Transfer.* **110,** 321-328.

Iacavides, H. 1998 Computation of flow and heat transfer through rotating ribbed passages. *Int. J. Heat and Fluid Flow.* **19,** 393-400.

Korotky, G. J. & Taslim, M. E. 1998 Rib Heat Transfer Coefficient Measurements in a Rib-Roughened Square Passage. *J. Turbomachinery.* **120,** 376-385.

Lien, F. S.& Durbin, P. A. 1996 Non-linear $k-\epsilon-v^2$ modeling with application to high-lift. *Proceedings of the 1996 Summer Program.* Center for Turbulence Research NASA Ames/Stanford University, 5-22**.**

Liou, T. M., Hwang, J. J. & Chen, S. H. 1993 Simulation and measurement of enhanced turbulent heat transfer in a channel with periodic ribs on one principal wall. *Int. J. Heat Mass Transfer.* **36**(2)**,** 507-517.

Metzger, D. E., Bunker, R. S. & Chyu, R. K. 1989 Cavity Heat Transfer on a Transverse Grooved Wall in a Narrow Flow Channel. *J. Heat Transfer.* **111,** 73-79.

Rau, G., Cakan, M., Moeller, D. & Arts, T. 1998 The Effect of Periodic Ribs on the Local Aerodynamic and Heat Transfer Performance of a Straight Cooling Channel. *J. Turbomachinery.* **120,** 368-375.

Shabany, Y. & Durbin, P. A. 1997 On Explicit Algebraic Scalar Flux Approximation. *AIAA J.* **35**(6)**,** 985-989.

Simoneau, R. J. & Simon, F. F. 1992 Progress towards understanding and predicting heat transfer in the turbine gas path. *Int. J. Heat and Fluid Flow.* **14**(2)**,** 106-128.

Speziale, C. 1997 Comparison of Explicit and Traditional Algebraic Stress Models of Turbulence. *AIAA J.* **35**(9)**,** 1506-1509.

Stephens, M. A. 1995 Computation of Flow and Heat Transfer in a Rectangular Channel with Ribs. *AIAA Paper 95-0180.*

Wadia, A. R. & Booth, T. C. 1982 Rotor-Tip Leakage:Part II-Design Optimization Through Viscous Analysis and Experiment. *ASME J. Engr. for Power.* **104,** 162-169.

Wolfshtein, M. 1969 The Velocity and Temperature Distribution of One-Dimensional Flow with Turbulence Augmentation and Pressure Gradient. *Int. J. Heat Mass Transfer.* **12,** 301-318.